THEORITICAL STUDY OF QUANTUM TRANSPORT

M.Sc. Thesis

By LAKHYANATH KULI Roll no. 2303151020





INDIAN INSTITUTE OF TECHNOLOGY INDORE

CANDIDATE'S DECLARATION

I hereby certify that the work which is being presented in the thesis entitled **Theoritical study of quantum transport** in the partial fulfillment of the requirements for the award of the degree of **MASTER OF SCIENCE** and submitted in the **DISCIPLINE OF PHYSICS**, Indian Institute of Technology Indore, is an authentic record of my own work carried out under the supervision of **Dr.Bivas Dutta**, **Assistant Professor**, **Department of physics**, **IIT Indore**.

The matter presented in this thesis has not been submitted by me for the award of any other degree of this or any other institute.

19/05/25

Convener, DPGC

Signature of the student with date (Lakhyanath kuli)

This is to contify that the above statement made by the condidate is convect

This is to certify that the above statement made by the candidate is correct to the best of my/our knowledge.

Biras Dutta

Signature of the Supervisor of

M.Sc. thesis #1 (with date)

(Dr.Bivas Dutta)

.....

Birasputta

Signature(s) of Supervisor(s) of MSc thesis

Date: 19/05/25 Date: 20-05-25

Acknowledgment

First and foremost, I would like to express my heartfelt gratitude to my supervisor, Dr. Bivas Dutta, for his constant guidance, valuable suggestions, and encouragement throughout the course of this project. His patience, deep knowledge, and support were crucial for the successful completion of my thesis.

I am also thankful to the faculty members and staff of the Discipline of Physics at IIT Indore, whose lectures, advice, and facilities have contributed significantly to my academic and research growth during the MSc program.

I sincerely thank the Departmental Project Evaluation Committee (PSPC members) for their constructive feedback and for evaluating my work with attention and care.

I am grateful to my friends and batchmates, who have always been supportive, and whose company made the journey enjoyable and less stressful.

Special thanks to my family for their unconditional love, encouragement, and support throughout my academic life. Their belief in me gave me the strength to stay focused and complete this work.

Finally, I thank the Indian Institute of Technology Indore for providing an excellent environment for learning and research, and for the opportunities that helped me grow both personally and professionally.

Abstract

This thesis presents a theoretical study of electron transport in small electronic devices, especially Single-Electron Transistors (SETs) and quantum dots (QDs). At very small sizes, traditional electrical behavior changes, and new effects like tunneling, charge quantization, and Coulomb blockade become important. These effects help explain how electrons move one at a time in controlled ways, which is useful for building energy-efficient and highly sensitive devices.

The work starts by examining SETs with metallic islands, where electron flow is blocked or allowed based on the charging energy and the applied gate voltage. Then, it focuses on quantum dots, which are even smaller regions where electrons are confined, leading to discrete energy levels. The study shows how gate voltage can tune the energy levels and control the flow of electrons through the device. The resulting patterns, called Coulomb diamonds, are explained using simple energy models.

Later sections explore more complex processes such as co-tunneling and the Kondo effect. These occur when electrons interact strongly or when regular tunneling is blocked. These processes change how current flows through the device, especially at very low temperatures.

The thesis also discusses thermal transport in Single-Electron Devices, where not only charge but also heat is carried by electrons. It explains how heat transfer is influenced by factors like charging energy, gate voltage, and temperature. The study shows that under certain conditions, classical laws such as the Wiedemann–Franz law do not hold. These findings are important for understanding energy flow in nanoscale systems and can help in designing low-power and thermally efficient devices.

The models and concepts discussed in this work are supported with mathematical analysis and diagrams to improve understanding. Although the study is theoretical, it connects closely with experimental observations. Overall, this thesis provides a strong foundation for understanding electron and thermal transport in nanoscale systems and supports future research in nanoelectronics and device design.

Contents

| 1 | Qua | ${f antum}$ charge transport through Single Electron transistor (SE) | \mathbf{ET}) | 6 |
|--------------|-----|--|-----------------|---|
| | 1.1 | SET with metallic island: | 6 | |
| | 1.2 | Charge Transport | 7 | |
| | 1.3 | Coulomb diamond | 9 | |
| 2 | SET | With Quantum Dot | 10 | |
| | 2.1 | Charge Transport | 10 | |
| | | 2.1.1 Influence of gate voltage on charge transport in QD | 11 | |
| | 2.2 | Coulomb diamond analysis | 12 | |
| | | 2.2.1 Linear equations corresponding to Coulomb diamond \dots | 13 | |
| | 2.3 | Charging Energy and Diamond Extents | 15 | |
| 3 | Hig | gher-Order Tunneling | 16 | |
| | 3.1 | Regimes in the Co-tunneling process | 16 | |
| | 3.2 | Stability diagram | 18 | |
| 4 | Kor | ndo effect | 20 | |
| | 4.1 | Fundamental Description of the Kondo Effect in Metals | 20 | |
| | 4.2 | The Kondo Effect in Quantum Dots | 21 | |
| 5 | The | ermal transport in single Electron Device | 24 | |
| | | 5.0.1 High Temperature Regime $(k_BT = E_C/2)$ | 25 | |
| | | 5.0.2 Intermediate Temperature Regime $(k_B = E_C/10)$ | 25 | |
| | | 5.0.3 Low-Temperature Regime $(k_BT = E_C/40)$ | 26 | |
| | 5.1 | Temperature Dependence of the Lorentz Ratio | 26 | |
| | 5.2 | Experiments on Thermal transport through SETs | 27 | |
| | | 5.2.1 Thermoelectric Conductance Characteristics of a SET | 29 | |
| \mathbf{A} | Der | ivation of Energy cost for tunneling | 33 | |
| | | A.0.1 Total charging energy: | 33 | |
| В | Der | ivation of the chemical potential of Quantum Dot(QD): | 36 | |

C Derivation of the expression of the slope of coulumb diamond: 38

List of Figures

| 1.1 | from [7]) | 9 |
|-----|---|----|
| 2.1 | Energy level schematic of a quantum dot: (a) illustrating the Coulomb blockade regime, and (b) depicting single-electron tun- | |
| | neling events | 11 |
| 2.2 | A Coulomb diamond plot depicts electron transport through a quantum dot as a function of the bias voltage V_b and the dimensionless gate voltage n_g . The diamond-shaped shaded areas represent regions of Coulomb blockade, where electron flow is inhibited. Outside these regions, sequential tunneling is allowed due to favorable energy conditions. The insets illustrate the alignment of energy levels between the electrochemical energies of the source (μ_s) and drain (μ_d) terminals and the electrochemical potentials $\mu(N)$, $\mu(N+1)$, etc., of the confined region (quantum dot), emphasizing resonant tunneling conditions and transitions between | |
| | charge states at the diamond boundaries | 14 |
| 3.1 | Conductance diagram of the quantum dot (QD) showing the influence of higher-order tunneling processes across multiple electron occupancy regimes (Adapted from [3]) | 17 |
| 2.0 | | 11 |
| 3.2 | Stability diagram plotted in the plane of the source-drain voltage V_{sd} and gate voltage V_g .(Adapted from [3]) | 18 |
| 4.1 | Schematic depiction of an impurity's unpaired spin embedded in a metal, interacting with the mobile spins of the conduction electrons. When the temperature is above the characteristic Kondo temperature T_K , only a small number of conduction electron spins are involved. However, below T_K , the impurity spin becomes completely screened by the surrounding delocalized spins, resulting in the formation of a spin-compensating region known as the Kondo | |
| | cloud | 21 |

| 4.2 | Energy diagram of the quantum dot (QD) under Kondo correla- | | | |
|-----|--|-----|--|--|
| | tions at a temperature $T < T_K$ | 22 | | |
| 5.1 | Gate voltage dependence of Lorentz ratio (Adapted from [14]) | 25 | | |
| 5.2 | Temperature dependence of Lorentz ratio (Adapted from [14]) | 26 | | |
| 5.3 | False-colored SEM image of the Asymmetric design[6] [pp.86-87] | | | |
| | device. One of the blue colored component is the thermometer (ex- | | | |
| | treme right side) and the other (extreme left side) is the cooler/heater. | .In | | |
| | the magnified image (left) red color indicates source ,yellow is the | | | |
| | metallic island and green is the drain. (Adapted from $[5]$) | 28 | | |
| 5.4 | The left plot illustrates the variation of the electronic temperature | | | |
| | T_e of sample B $(R_N = 52 \Omega)$ as a function of the cooler bias voltage | | | |
| | $V_{\rm cool}$. The right plot shows the dependence of T_e on the gate | | | |
| | voltage: the top graph corresponds to the heating regime, while | | | |
| | the bottom graph represents the cooling regime. (Adapted from [5] | 29 | | |
| 5.5 | The thermal conductance (represented by blue dots) and charge | | | |
| | conductance (depicted by green dots) of the SET are shown at a | | | |
| | bath temperature of 132 mK (left, sample A) and 152 mK (right, | | | |
| | sample B), measured relative to the conductances observed in the | | | |
| | gate-open configuration. (Adapted from [5]) $\ \ldots \ \ldots \ \ldots$ | 30 | | |
| | | | | |

Introduction

In recent years, the miniaturization of electronic components has led to growing interest in how quantum effects influence charge and heat transport at the nanoscale. Devices such as Single-Electron Transistors (SETs) and quantum dots (QDs) have become important in this field because they allow control over individual electrons.

This project explores how effects like tunneling and Coulomb blockade affect electron transport in SETs. At very small scales, classical models no longer apply, and quantum behavior becomes dominant. In metallic islands, energy levels are nearly continuous, and transport is mainly governed by charging energy. In contrast, quantum dots exhibit discrete energy levels due to confinement, resulting in more complex and tunable transport behavior.

The thesis also discusses higher-order effects such as co-tunneling and the Kondo effect. These become relevant when simple sequential tunneling is blocked, especially at low temperatures. In such cases, electrons can still pass through the device using virtual intermediate states or through spin interactions, altering the overall conductance.

In addition to charge transport, this study also looks at thermal transport in Single-Electron Devices, where electrons carry heat as well as charge. Heat flow in these systems depends on factors like gate voltage, temperature, and charging energy. At the nanoscale, the usual rules that relate heat and charge transport—such as the Wiedemann–Franz law—may no longer apply due to strong electron interactions. Understanding this behavior is important for designing energy-efficient and low-power devices.

Overall, this work provides a theoretical understanding of both charge and heat transport in nanoscale systems. It connects fundamental physics with potential applications in nanoelectronics, and may help guide the design of future advanced devices.

Chapter 1

Quantum charge transport through Single Electron transistor(SET)

A single-electron transistor (SET) is a tiny electronic device that controls the flow of one electron at a time. It works like a regular transistor, which can turn electrical signals on or off, but at a much smaller scale. The SET uses a special effect called "quantum tunneling" where electrons can pass through barriers even if they seem unable to.

Why do we need SET over regular transistors? We need Single-Electron Transistors (SETs) over regular transistors because they offer precise control of individual electrons, making them ideal for highly sensitive and low-power applications, especially at the nanoscale. Unlike regular transistors, which struggle with leakage and heat as they shrink, SET usages quantum effects like tunneling and energy quantization to operate efficiently at extremely small sizes. This makes them crucial for future technologies such as quantum computing and ultra-sensitive sensors, where traditional transistors face limitations in performance and scalability. Single electron transistors (SETs) can be implemented using either metallic islands or quantum dots, each offering unique ways to control electron flow at the nanoscale.

1.1 SET with metallic island:

Metallic islands are small conducting regions separated by insulating barriers, known as tunnel junctions, from the source and drain electrodes. Due to quantum tunneling, metallic islands allow electrons to pass through only one at a time, making them crucial for applications requiring precise control of electron flow.

At room temperature, thermal fluctuations provide electrons with sufficient energy to surpass the Coulomb blockade barrier (the regime of zero conduction), leading to continuous rather than discrete tunneling events. To overcome this, the thermal energy k_BT must remain much smaller than the charging energy $E_c = \frac{e^2}{2C}$, where e is the electron charge and C is the capacitance of the island. The charging energy represents the energy needed for an electron to overcome Coulombic repulsion from the other electrons in the island. Metallic islands, generally tens to hundreds of nanometers in size, exhibit a quasi-continuous energy spectrum due to their relatively large dimensions. In contrast, quantum dots(we'll see in the next chapter2), which are much smaller-often only a few nanometers exhibit strong quantum confinement, resulting in discrete and well-separated energy levels. We can think of the Quantum dot as a particle in a box, which restricts electron movement and forces them into specific quantized states.

1.2 Charge Transport

In a SET, electron transport across the metallic island is mainly governed by the Coulomb blockade and precise control over individual tunneling processes. The metallic island, positioned between the source and drain lead and isolated by thin insulating barriers, acts as a confined region where individual electrons can tunnel in and out under specific conditions. The transport of electrons through the metallic island is influenced primarily by two factors: charging energy and thermal energy. Due to the small size, the energy required to add an additional electron, known as the charging energy $E_c = \frac{e^2}{2C}$ creates an electrostatic barrier that prevents electrons from freely entering the island unless a certain energy threshold is met. When the thermal energy k_BT (where k_B is Boltzmann's constant and T is temperature) is lower than the charging energy, the island is in a regime of Coulomb blockade, effectively preventing electron transport at low gate voltages (Dark blue region in Fig.1.1). To overcome this blockade, we use the gate voltage (V_q) that influences the electrostatic potential of the metallic island. By adjusting the gate voltage, the Coulomb blockade can be lifted periodically, allowing an electron to tunnel onto the island from the source lead, and then from the island to the drain lead. This tunneling occurs in a controlled discrete manner, with electrons moving one by one, as the gate voltage cycles through the conditions that align with the charging energy requirements. This results in Coulomb oscillations in the current, with each peak (Conductance) representing a single-electron tunneling event.

Since the size of the metallic island is in the range of nanoscale, which is small enough to show quantum effect like the tunneling, which leads to the flow of charge, but not small enough like a Quantum dot for its energy level to be discretized. So the island's energy depends only on the charge it holds, its capacitance(C), the surrounding electrostatic environment, and any gate voltages. Thus the electrostatic energy of the island is given by[?]

$$E_{\rm el} = \frac{(Ne)^2}{2C} - Ne\phi_{\rm g} \tag{1.1}$$

where: $\frac{(Ne)^2}{2C}$ is the coulomb charging energy for N electron, which is the energy required to add N electron into the QD. $Ne\phi_g = E_g$ is the potential energy of the charge(Ne)of the QD due to the gate voltage(V_g).

So, in the above equation, we can see that because of the non-discreteness of the energy level the energy due to the discrete level is not included, which will be included in the case of a Quantum dot. In a metallic island, the energy levels are not typically discrete. They usually have a high density of states, meaning that the energy levels are effectively continuous due to the large number of available electron states. This is because the island contains a large number of atoms, leading to closely spaced energy levels, which can be treated as a continuum. So, no strict energy quantization for individual electron levels occurs. As a result, an electron in the source can tunnel into the metallic island without being required to match a specific discrete energy level E(N+1) (the energy state associated with an extra electron within the quantum dot).

So, thus the energy cost (required) for tunneling into (+) or out (-) of the island, $\Delta E_{i,n}^{\pm}$, is determined by the surplus electron count and the applied voltage across the island and is given by [6]: (Detail derivation in Appendix A).

$$\Delta E_{i,n}^{\pm} = \pm 2E_c \left(n - n_g \pm \frac{1}{2} \right) \pm eV_{b,i}$$
 (1.2)

Where: $E_c = \frac{e^2}{2C}$ is the charging energy, which is significant in small islands. $n_g = \frac{C_g V_g}{e}$ is the gate-induced charge, where C_g is the gate capacitance, and V_g is the gate voltage. n is the number of electrons in the island. $C = C_1 + C_2 + C_g$ is the total capacitance, summing the capacitances between the island and the source electrode, drain electrode, and gate terminal, respectively. $V_{b,i} = k_i V_b$ is the portion of the externally applied potential difference dropped across each tunnel junction i, with $k_i = \frac{\tilde{C}}{C_i}$, where $\tilde{C} = \frac{C_1 C_2}{C_1 + C_2}$ is the equivalent capacitance.

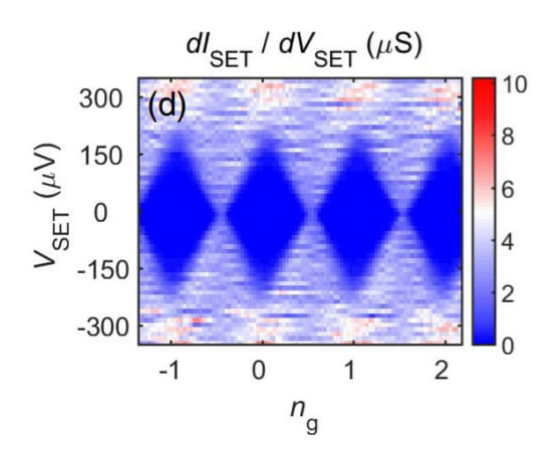


Figure 1.1: The charge stability diagram for an SET(Metallic island)(Adapted from [7])

1.3 Coulomb diamond

In a SET device, the transfer of electrons between the leads and the central island occurs under specific energy conditions controlled by the system's electrostatic configuration.; tunneling occurs only when the energy cost is low enough such that the chemical potential of $Dot(\mu_d)$ aligns with or lies between the source and drain lead's Fermi level. When this tunneling take place we get current which can be seen as a light blue and red region in Fig.1.1. When the energy of the electron is not enough for tunneling then this creates Coulomb blockade regions where charge transport is blocked, forming Coulomb diamonds (Dark blue region in Fig.1.1) in a plot of gate voltage V_g versus bias voltage V_b . In the plot $n_g = \frac{C_g V_g}{e}$. So, $n_g \propto V_g$. Where, n_g is the average occupancy number of electrons in the island. Within each Coulomb diamond, the metallic island maintains a fixed and stable number of electrons. However, at the charge degeneracy points the intersections between adjacent diamonds—the island becomes energetically favorable to fluctuate between two neighboring charge states. The dimensions of the Coulomb diamonds are governed by the charging energy E_c . Along the n_g (or gate voltage V_g) axis, the diamonds span a range of $\frac{2E_c}{e}$, while along the bias voltage V_b axis, their extent is $\frac{E_c}{e}$.

Chapter 2

SET with Quantum Dot

In a SET based on a quantum dot(QD), charge transport occurs through the quantum tunneling of individual electrons same as that of metallic island. A quantum dot is in the nanoscale region much smaller than that of the metallic island, so it confines electrons, acting like an artificial atom with discrete energy levels. The quantum dot is located between two metallic leads (source and drain) and is connected to a third terminal, the gate, which controls the potential of the dot. As a result, it controls the position of the energy level of the Dot, which the tunneling electron can occupy. It is separated from the leads by tunneling barriers, which are thin insulating layers that electrons can quantum mechanically tunnel through.

2.1 Charge Transport

Charge conduction across a nanoscale quantum system involves the process of electrons moving between the quantum device and leads, typically governed by quantum tunneling, energy quantization, and electrostatic phenomena such as Coulomb repulsion. Unlike a continuous band of energy levels found in larger materials like the metallic island, a quantum dot has discrete, quantized energy levels due to its small size and quantum confinement effects. Because of which the total electrostatic energy of the Quantum Dot (QD) depends not only on the charge in it and the gate voltage (V_g) but also on the Sum of the energy of the discrete level in the QD where the electron are occupied.

So, the expression of the total energy of the QD is given by [6]:

$$E_{\text{total}}(N) = \sum_{p} \varepsilon_{p} + E_{\text{el}}(N)$$
 (2.1)

where:

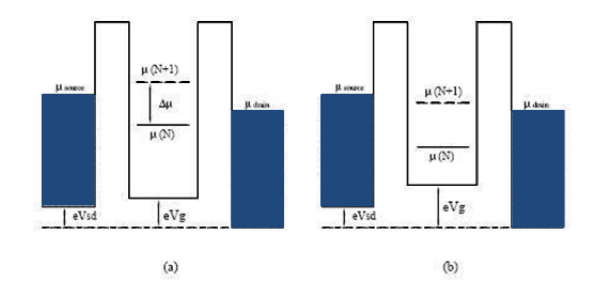


Figure 2.1: Energy level schematic of a quantum dot: (a) illustrating the Coulomb blockade regime, and (b) depicting single-electron tunneling events.

- $E_{\rm el}(N) = \frac{(Ne)^2}{2C} Ne\phi_{\rm ext}$ is the electrostatic energy of the QD due to its charge in it and the gate voltage. $(\phi_{ext} = \sum \frac{C_i}{C} V_{ext,i})$ is the potential due to the external reservoirs or gates.)
- The expression $\sum_{p} \varepsilon_{p}$ represents the total energy accumulated from all occupied discrete energy levels.

The term $\sum_{p} \varepsilon_{p}$ accounts for the total quantum mechanical energy contributed by electrons occupying the discrete energy levels within the quantum dot.

The energy difference between the quantum dot and the Fermi level of the leads defines the energy required for adding an extra electron into the quantum system, which can be expressed as [11]:

$$\mu(N) = E_{\text{total}}(N+1) - E_{\text{total}}(N)$$
(2.2)

Substituting from earlier expressions(3.1), we get(Detail derivation in Appendix B):

$$\mu(N) = \varepsilon_{N+1} - e\phi_{\text{ext}} + \frac{(N+1/2)e^2}{C}$$
(2.3)

Here, ε_{N+1} denotes the energy of the (N+1)th discrete electron level, while $\frac{(N+\frac{1}{2})e^2}{C}$ represents the Coulomb energy required to add the (N+1)th electron. Together, these terms define the total energy cost associated with the tunneling of an additional electron into the quantum dot.

2.1.1 Influence of gate voltage on charge transport in QD

Charge flow through a nanoscale quantum system (QD) is regulated through the applied gate voltage (V_g) , which adjusts the discrete energy levels within the QD via modulation of its chemical potential (μ_d) . This adjustment influences the electron tunneling criteria relative to the connected source and drain terminals.

The charge induced on the QD by the gate voltage is given by:

$$Q_{\text{ext}} = C_g V_g = n_g e \tag{2.4}$$

where: C_g is the capacitance between the QD and the gate, V_g is the gate voltage, $n_g e$ is the charge induced on the QD.

The tunneling condition depends on the chemical potential of the $QD \mu(N)$. When $\mu(N) = 0$ (i.e. when the fermi levels of the leads and the DOT are aligned), the tunneling energy cost is zero. So, the equation (2.3) becomes:

$$e\phi_{\text{ext}} = \epsilon_{N+1} + \frac{(N+1)e^2}{2C}$$
 (2.5)

Substituting ϕ_{ext} in terms of gate voltage yields:

$$\phi_{\text{ext}} = \frac{Q_{\text{ext}}}{C} = \frac{C_g V_g}{C} = \alpha V_g \tag{2.6}$$

where $\alpha = \frac{C_g}{C}$ is the gate coupling factor.

The tunneling condition becomes:

$$e\alpha V_g = \epsilon_{N+1} + \frac{(N+1)e^2}{2C} \tag{2.7}$$

Thus, the conductance of the QD oscillates with V_g , reaching a maximum when the condition is satisfied. Each conductance peak corresponds to the addition of one electron to the QD.

Periodicity of Conductance Oscillations

The periodicity of conductance peaks is determined by the energy required to add an electron ($E_{\rm add} \text{or} \Delta \mu$) Fig.2.1, given by:

$$E_{\text{add}} = e\alpha \Delta V_q = \delta E + 2E_c \tag{2.8}$$

where δE denotes the energy spacing between adjacent single-particle energy levels, $2E_c$ is the Coulomb charging energy, α is the gate coupling factor and ΔV_g is the gate voltage spacing between conductance peaks.

This equation explains the periodic nature of the conductance oscillations in QDs, with each period corresponding to the addition of one electron.

2.2 Coulomb diamond analysis

In Fig.2.2, the distinct diamond-like patterns indicate regions of charge stability and are typically identified by the term Coulomb blockade diamonds[8, 13]. Within these regions, charge transport is suppressed due to the Coulomb blockade. The junction of two neighboring diamonds marks the degeneracy point in the charge state, a condition under which the energy required for additional

electron occupancy becomes negligible. Features beyond the Coulomb blockade area reflect the quantized energy states within the quantum dot.

In the figure (2.2), the green lines running parallel to the edges of the coulomb diamond are the excited state corresponding to a certain ground state to which it intersects.

The energy level spacing δE can be determined from the bias voltage difference δV_b .

If **red lines** appears then it means that at certain biasing voltage V_b the ground and the excited state comes under the bias window.

2.2.1 Linear equations corresponding to Coulomb diamond

The current-voltage (I-V) characteristics of the quantum dot display sharp steps whenever the dot's chemical potential μ_d matches the energy level of the leads.

The Coulomb diamonds arise from the alignment conditions of the dot's chemical potential with the leads, i.e. the degenerate state. These are described by the linear equations (Detailed derivation in Appendix Csection 1):

$$V_b = \beta V_q + k, \tag{2.9}$$

$$V_b = -\beta' V_g + k, \tag{2.10}$$

where, V_b is the bias voltage, and V_g is the gate voltage. β is the slope of the positive edge of the coulomb diamond which corresponds to the boundary condition i.e when the chemical potential(μ_s) of source(lead 1) align with chemical potential (μ_{dot}) of QD. And on the other hand β' is the slope of the negative edge of the coulomb diamond which corresponds to the another boundary condition i.e when the chemical potential(μ_d) of drain(lead 2) align with chemical potential (μ_{dot}) of QD.

The slopes β and β' are given by:

$$\beta = \frac{C_g}{C_d + C_g}, \quad \beta' = \frac{C_g}{C_s}, \tag{2.11}$$

Here, C_g denotes the capacitance linking the quantum dot and the gate, C_s serves as the capacitance linking the quantum dot and the source, and C_d corresponds to the capacitance linking the quantum dot and the drain. The total capacitance of the system is given by:

$$C = C_s + C_d + C_g.$$

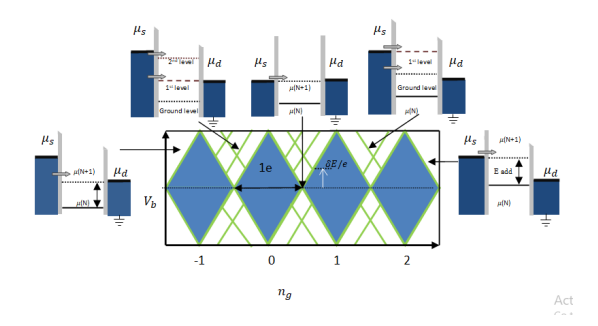


Figure 2.2: A Coulomb diamond plot depicts electron transport through a quantum dot as a function of the bias voltage V_b and the dimensionless gate voltage n_g . The diamond-shaped shaded areas represent regions of Coulomb blockade, where electron flow is inhibited. Outside these regions, sequential tunneling is allowed due to favorable energy conditions. The insets illustrate the alignment of energy levels between the electrochemical energies of the source (μ_s) and drain (μ_d) terminals and the electrochemical potentials $\mu(N)$, $\mu(N+1)$, etc., of the confined region (quantum dot), emphasizing resonant tunneling conditions and transitions between charge states at the diamond boundaries.

Capacitive Coupling: The capacitive coupling between the dot and the source/drain can be extracted from the slopes of the Coulomb diamond edges. This asymmetry is described by the ratio C_d/C_s (Detail derivation in Appendix C section 2):

$$\frac{C_d}{C_s} = \beta' \left(\frac{1}{\beta} - 1\right). \tag{2.12}$$

If the ratio $\frac{C_d}{C_s} = 1$, the coupling is symmetric, meaning the quantum dot is equally coupled to both the source and the drain. If $\frac{C_d}{C_s} > 1$, the quantum dot is more strongly coupled to the drain. If $\frac{C_d}{C_s} < 1$, the quantum dot is more strongly coupled to the source.

Gate Coupling Factor (Lever Arm): The parameter α , often termed the lever-arm, plays a crucial role in linking variations in the quantum dot's chemical potential $\Delta\mu$ with corresponding changes in the gate voltage ΔV_g . This factor can be directly obtained from the slopes β and β' as (Detail derivation in Appendix C section 30):

$$\alpha = \frac{C_g}{C} = \frac{1}{\left(\frac{1}{\beta} + \frac{1}{\beta'}\right)} \tag{2.13}$$

2.3 Charging Energy and Diamond Extents

One can estimate E_c by examining the extent of the diamond-shaped stability regions plotted against both gate and bias voltages in transport measurements of a quantum-confined structure. The period of conductance oscillations corresponds to the energy required to add an electron, and this is defined as:

$$E_{\text{add}} = 2E_c + \delta E \tag{2.14}$$

where, δE denotes the separation among the quantized energy levels within the confined QD.

Horizontal extent: The horizontal extent of the Coulomb diamond (along the V_q -axis in Fig.2.2) is related to the addition energy by

$$\Delta V_g = \frac{E_{\text{add}} C_g}{\alpha e} \tag{2.15}$$

This equation tells us that the horizontal width ΔV_g of the coulomb diamond provides information about the addition energy E_{add} in relation to the gate capacitance C_g and the lever arm α . In other words, by measuring the span of the Coulomb blockade region along the V_g -axis, we can estimate the electron addition energy of the quantum dot. A larger ΔV_g means a larger addition energy which indicates either a high Coulomb charging energy E_{add} , which indicates either a high Coulomb charging energy E_c , large quantum confinement (leading to large δE) or both.

Vertical extent: Similarly, the height of the diamond-shaped region in the V_b direction, as shown in Fig. 2.2, offers an alternative way to determine the addition energy.:

$$\Delta V_b = \frac{E_{\text{add}}}{e}.\tag{2.16}$$

This equation shows that the vertical height ΔV_b of the Coulomb diamond is proportional to the addition energy E_{add} . In other words, by measuring the height of the Coulomb diamond along the V_b axis, we can directly estimate the addition energy. A larger ΔV_b indicates a larger addition energy. This means that a larger bias voltage is needed to overcome the Coulomb blockade and allow electron transport.

Chapter 3

Higher-Order Tunneling

In contrast to sequential tunneling discussed in the previous Chapter2, where single electrons tunnel one by one through the quantum dot (QD) or metallic island, co-tunneling represents a higher-order process that dominates in the Coulomb blockade regime [10].. When sequential tunneling is blocked, second-order cotunneling allows charge transport through the simultaneous tunneling of multiple electrons across the system. This process involves the quantum dot briefly occupying virtual intermediate states, which are not directly observable but enable the system to bypass the Coulomb blockade. The nature of co-tunneling depends strongly on the coupling strength between the leads and the quantum dot or metallic island. Co-tunneling is classified into elastic and inelastic processes. In elastic co-tunneling, an electron tunnels in and out of the quantum dot or metallic island, leaving it in its ground state. This process dominates at low bias voltages, where the applied energy does not excite the system. In contrast, inelastic co-tunneling occurs when the quantum dot is left in an excited state after the tunneling event. This requires the external bias $|eV_b|$ to exceed the energy gap δE between the ground and excited states of the dot. Consequently, inelastic co-tunneling sets in at higher bias voltages, contributing additional transport channels.

3.1 Regimes in the Co-tunneling process

There are two regimes: one consists of elastic processes only, and the other includes elastic and inelastic contributions.

Elastic-only regime: Only elastic co-tunneling occurs. This typically happens at low-bias voltages because the energy the bias provides is insufficient to excite the quantum dot.

Elastic and inelastic regimes: As the bias voltage increases and surpasses

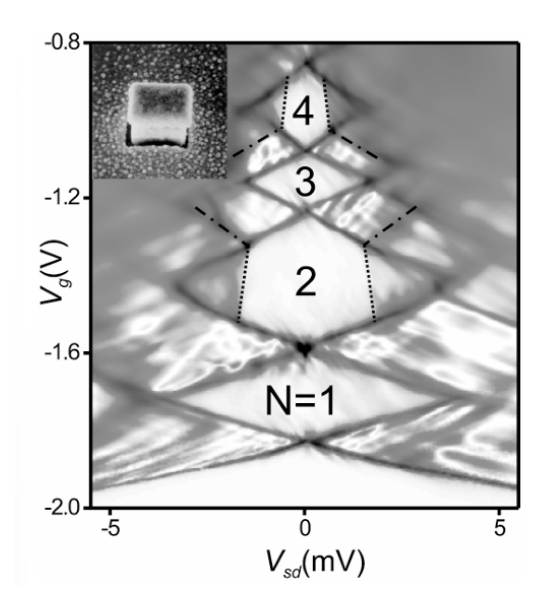


Figure 3.1: Conductance diagram of the quantum dot (QD) showing the influence of higher-order tunneling processes across multiple electron occupancy regimes(Adapted from[3]).

a certain threshold (the excitation energy of the dot), both elastic and inelastic co-tunneling can occur. Inelastic co-tunneling becomes possible because the bias now supplies sufficient energy to elevate the quantum dot to an excited state with an elevated energy level.

These two regime can be seen in the coulomb diamond diagram fig1. In the region where the N(average occupancy no.) = odd, the 1st regime can be seen, and in N=even, the 2nd regime can be seen. Both these co-tunneling processes are virtual processes, which means that the electron that tunnels through the dot does not actually occupy an energy level in the quantum dot for a measurable amount of time. It tunnels through a virtual intermediate state.

Transition between the Regimes: The transition between these Regimes an be sharper than the characteristic lifetime broadening of the dot's energy levels[2]. It means that this transition is governed by a specific threshold in the applied bias voltage, marking the onset of inelastic co-tunneling. In this regime (typically observed in the Coulomb diamond region where the electron number N is even, which is control by the gate voltage), the quantum dot make transitions from only elastic processes to allowing both elastic and inelastic co-tunneling. The bias voltage threshold corresponds to the first excitation energy of the confined quantum system, defined as the separation in energy (δE) from the ground state to its first excited configuration.

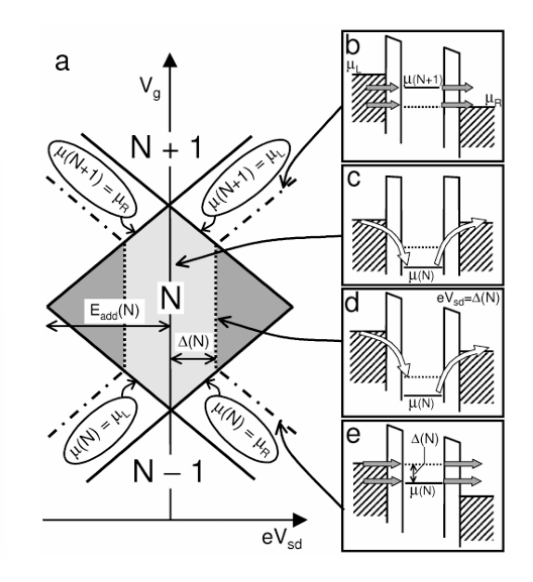


Figure 3.2: Stability diagram plotted in the plane of the source-drain voltage V_{sd} and gate voltage V_q .(Adapted from [3]).

3.2 Stability diagram

The stability diagram (Fig. C) of a generic quantum dot can be obtained by plotting the differential conductance $\frac{dI}{dV_{sd}}$ as a function of the bias voltage V_{sd} and the gate voltage V_q .

The stability plot depicts electron transport behavior in a quantum dot, mapped against variations in both source—drain voltage V_{sd} and applied gate voltage V_g , emphasizing Coulomb blockade effects and transitions among various tunneling regimes.

(a) Stability Diagram Overview:

The Coulomb diamonds (grey regions) represent the Coulomb blockade, where no current flows due to insufficient required energy to introduce a further electron onto the confined quantum system. Within each diamond, the QD maintains a fixed electron number (N, N + 1, N - 1). The slanted edges of the diamonds correspond to the alignment of QD energy levels with the Fermi levels of the leads, allowing sequential tunneling (first-order transport). Vertical dotted lines inside the diamonds indicate the onset of inelastic co-tunneling, where the bias voltage (eV_{sd}) provides enough energy to excite the QD.

Transport Mechanisms:

1. Sequential Tunneling Through Ground and Excited States (Figures 3.2 b, e):

(b) and (e) represent sequential tunneling via the first excited energy level of the quantum dot. When the QD energy levels align with the Fermi levels of the leads, electrons tunnel through the dot one by one, either via the ground state or the excited state. These processes occur outside the Coulomb blockade region, along the edges of the diamonds.

2. Elastic Co-Tunneling (Figure 3.2 c):

Inside the Coulomb blockade (light grey regions in Fig.3.2), transport occurs via second-order processes. One electron virtually tunnels into the QD while another simultaneously exits, so that the quantum dot remains in its ground energy state. This mechanism provides finite conductance within the diamonds without exciting the QD, contributing to charge transport in the blockade region.

3. Inelastic Co-Tunneling (Figure 3.2 d):

At higher bias $(eV_{sd} \geq \Delta(N))$, the QD gains energy and transitions to an excited state. In this process, one electron tunnels out of the QD's ground state while another tunnels into an excited state, resulting in an energy difference $\Delta(N)$, corresponding to the first excited energy level of the quantum dot. This mechanism leaves the quantum dot occupying an excited energy level and is marked by vertical dotted lines in the diagram, as the process depends mainly on V_{sd} .

This diagram clearly shows how bias and gate voltages control the transport through a QD. Sequential tunneling governs regions outside the Coulomb diamonds, including transport through the excited states (Figures 3.2b, e). Meanwhile, co-tunneling dominates within the Coulomb blockade region, transitioning between elastic (ground state) and inelastic (excited state) regimes based on the bias energy.

Chapter 4

Kondo effect

4.1 Fundamental Description of the Kondo Effect in Metals

The Kondo effect originates from the interaction between a localized magnetic impurity (such as a spin- $\frac{1}{2}$ atom) and the conduction electrons in a metal. This interaction occurs via spin-exchange scattering, where the impurity spin couples with the spins of conduction electrons.

At high temperatures, scattering of conduction electrons off the impurity spin follows conventional magnetic scattering, causing the resistivity to decrease as the temperature decreases, resembling typical metallic behavior. However, as the temperature approaches the Kondo temperature T_K , a correlated spin-singlet state forms due to many-body interactions between the impurity spin and conduction electrons, as illustrated in Fig.4.1. This leads to enhanced scattering at low temperatures, resulting in an increase in resistivity.

This low-temperature regime is dominated by the Kondo resonance, characterized by a sharp peak in the density of states near the Fermi level, which increases scattering. The resistivity contribution due to the Kondo effect is approximately described as: [12]:

$$\rho(T) = \rho_o - c \ln\left(\frac{T}{T_k}\right) \tag{4.1}$$

indicating a logarithmic divergence as $T \to 0$, which is a key characteristic of Kondo effect. Where, T_K representing the characteristic energy scale at which the Kondo effect becomes significant. The concept of Kondo screening, initially explored in bulk metals, has since been extended to nanoscale systems like quantum dots, where it plays a reverse yet analogous role in enhancing conductance.

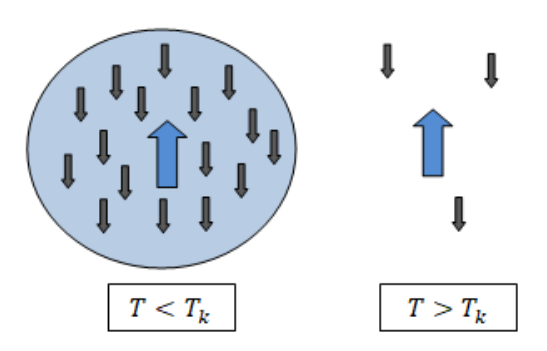


Figure 4.1: Schematic depiction of an impurity's unpaired spin embedded in a metal, interacting with the mobile spins of the conduction electrons. When the temperature is above the characteristic Kondo temperature T_K , only a small number of conduction electron spins are involved. However, below T_K , the impurity spin becomes completely screened by the surrounding delocalized spins, resulting in the formation of a spin-compensating region known as the Kondo cloud.

4.2 The Kondo Effect in Quantum Dots

Quantum Dots function as systems in which electrons experience confinement in all three spatial dimensions. Due to this confinement, the energy levels in a QD are discrete, and electron transport occurs primarily through tunneling. The Coulomb blockade regime dominates at low temperatures, where the addition of an extra electron to the dot is energetically unfavorable due to the charging energy. However, when the QD has an odd number of electrons, there is a net unpaired spin, analogous to the magnetic impurity in metals. Quantum dots (QDs) are artificial nanostructures in which electrons are confined in all three spatial dimensions. Due to this confinement, the energy levels in a QD become discrete, and electron transport primarily occurs via tunneling. At low temperatures, the Coulomb blockade regime dominates, where the addition of an extra electron to the dot is energetically unfavorable due to the charging energy.

However, when the QD contains an odd number of electrons, it hosts a net unpaired spin, analogous to a magnetic impurity in a metal. While the Kondo effect in metals leads to increased resistivity due to enhanced spin scattering, in QDs it manifests as an increase in conductance. In a QD with an unpaired spin- $\frac{1}{2}$, the interaction between the localized spin on the dot and the spins of tunneling electrons from the leads gives rise to a Kondo resonance. This resonance enhances the density of states near the Fermi level (see Fig.4.2), thereby opening an additional channel for electron tunneling and increasing the conductance, as described in Eq.4.2.

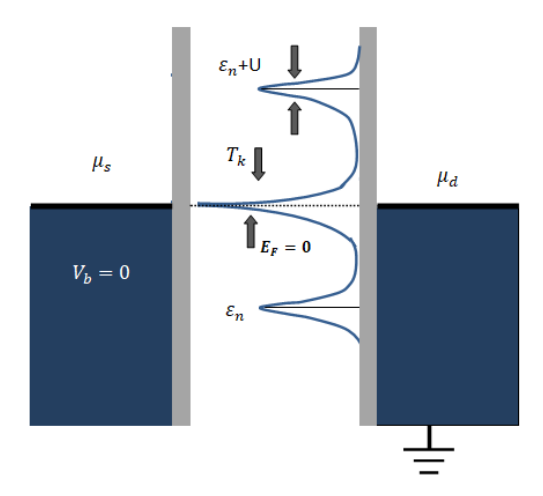


Figure 4.2: Energy diagram of the quantum dot (QD) under Kondo correlations at a temperature $T < T_K$.

As the temperature decreases, the conductance G increases due to the emergence of this resonance. The Kondo temperature T_K defines the energy scale of this effect, with the conductance reaching its maximum at T = 0.

An observed increase of conductance in QDs, arising from Kondo correlations, can be described by [9]:

$$G = \frac{2e^2}{h} \cdot \frac{T_K'^2}{T^2 + T_K^2} \tag{4.2}$$

where e is the electron charge, h is Planck's constant, and T_K is the Kondo temperature, $T'_k = T_k/\sqrt{2^{1/s} - 1}$ and $\frac{2e^2}{h} = G_0$ is the maximum conductance at T = 0. At $T \sim T_K$, the conductance reaches half of $G_0[1, 9]$, providing a clear experimental signature of the Kondo effect.

Kondo Temperature in QDs:

The Kondo temperature, which defines the energy scale for the formation of the Kondo resonance, can be expressed as:

$$T_K = \sqrt{\frac{\Gamma U}{2}} \exp\left(\frac{\pi \varepsilon_n(\varepsilon_n + U)}{\Gamma U}\right),$$

where: $\Gamma = \pi \rho V^2$ is the tunneling rate between the dot and the leads, U is the charging energy, ε_n is the energy level of the dot, ρ is the DOS in the leads.

The Kondo temperature increases with stronger tunneling coupling (Γ) and decreases with higher charging energy (U), illustrating the competition between Kondo screening and Coulomb blockade.

Co-Tunneling and Kondo Effect in Quantum Dots

In the Coulomb blockade regime, transport through the dot occurs via cotunneling, which involves the simultaneous tunneling of two electrons—one into the dot and one out of it. Co-tunneling processes can be:

1.Elastic Co-Tunneling: The total energy of the system remains unchanged. **2.Inelastic Co-Tunneling:** Energy is transferred, exciting the dot to a higher energy state.

For odd charge states $(N=1,3,\dots)$, the quantum dot contains an unpaired spin, and elastic co-tunneling dominates. Kondo resonance emerges when conduction electron spins in the leads couple with a localized spin, resulting in the formation of a spin-singlet state. This interaction increases the density of states at the Fermi level, enhancing conductance despite the elastic tunneling mechanism since $G \propto \mathrm{DOS}$ near Fermi level in Co-tunneling process.

For even charge states (N=2,4,...), there is no unpaired spin on the dot, and the Kondo effect is absent. Conductance occurs through purely elastic cotunneling for low biases $(eV_b < \delta E)$ and transitions to inelastic co-tunneling at higher biases.

Chapter 5

Thermal transport in single Electron Device

Thermal transport in a Single-Electron Transistor (SET) is fundamentally governed by tunneling electrons between reservoirs through tunnel junctions and the metallic island. This process leads to energy exchange, which results in heat flow. In a normal metal, electrical and thermal conductance are related by the Wiedemann-Franz law, which states that their ratio is a constant, known as the Lorenz number L_0 . However, in a SET, strong Coulomb interactions and quantum effects modify this relationship, leading to deviations of the Lorenz ratio (L/L_0) from the Wiedemann-Franz law, according to which $L/L_0 = 1$. Understanding these deviations helps us explore energy transport at the nano-scale. The transport of charge and heat in an SET occurs via sequential tunneling and co-tunneling processes, which is also known as higher-order tunneling. The heat current in the SET arises from the energy carried by tunneling electrons. When an electron tunnels from a lead onto the island, it extracts energy from the lead, while tunneling in the opposite direction injects energy into the lead. In the sequential tunneling regime, where E_C (charging energy)dominates over thermal energy($E_C > k_B T$), the Lorenz ratio is given by[14]:

$$\frac{L}{L_0} = 1 + \frac{\Delta_N^2}{4\pi k_B^2 T^2} \tag{5.1}$$

Where,

- Δ_N represents the energy required to add an electron to the Nth charge state, and is controllable through the gate voltage n_g .
- L_0 is the universal Lorenz number for normal metals.

Now, we discuss how the Lorenz ratio depends on gate-induced charge (n_g) which is controlled by gate voltage (V_g) and temperature (T).

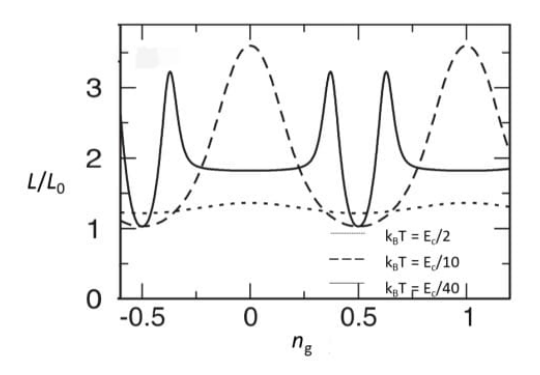


Figure 5.1: Gate voltage dependence of Lorentz ratio(Adapted from [14])

Gate Voltage Dependence of the Lorentz Ratio

The Lorenz ratio in a SET is strongly influenced by the applied gate voltage (V_g) , which controls the charge occupation of the island. Since charge transport in an SET is governed by Coulomb interactions, variations in the gate voltage modulate the tunneling rates and energy exchange, leading to deviations from the Wiedemann-Franz law.

The above plot (fig.5.1) shows the theoretical analysis of Lorenz ratio changes with gate-induced charge n_g for different temperatures. The three different curve correspond to different temperatures, we can divide the curves in the above plot into three regimes in terms of their operational temperature, which are High, Intermediate and low temperature regimes.

5.0.1 High Temperature Regime $(k_BT = E_C/2)$

At high temperatures, the Coulomb blockade is suppressed, meaning electrons can tunnel into the island regardless of the gate voltage since the thermal energy k_BT is much larger than the charging energy E_C (which is the energy required by electron to tunnel into the island). Gate voltage dependence is weak, and the Lorenz ratio is slightly greater than 1. Oscillations in the Lorenz ratio are suppressed because thermal excitations dominate over the charging effects. Even if thermal energy dominates over charging energy, the Lorentz ratio is still not one since charging energy is still present.

5.0.2 Intermediate Temperature Regime $(k_B = E_C/10)$

At intermediate temperature, Oscillations of L/L_0 appear, with maxima at integer values and minima at half-integer values. It follows a quadratic increase away from the charge degeneracy points($\Delta_N = 0$). At half-integer n_g , the Lorentz

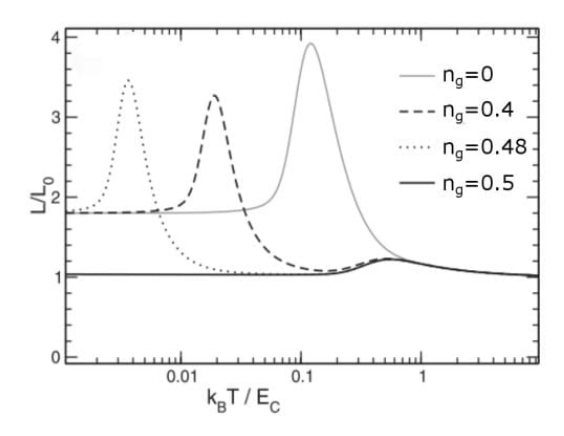


Figure 5.2: Temperature dependence of Lorentz ratio (Adapted from [14])

ratio becomes one (Wiedemann-Franz law holds). But at integer n_g , the charging energy gap Δ_N is quite high, only the electrons with enough energy can tunnel through. These electrons carry more thermal energy per electron, increasing the heat-to-charge transport ratio. As a result, L/L_0 increases significantly away from degeneracy points.

5.0.3 Low-Temperature Regime $(k_BT = E_C/40)$

The oscillations become more pronounced, with sharp peaks at the integer (n_g) and valleys at the half-integer (n_g) . The maximum value of L/L_0 increases significantly and saturates at 9/5(1.8) at off-degeneracy points. Sequential transport is exponentially suppressed. Higher-order co-tunneling processes dominate, where electrons tunnel via virtual intermediate states rather than direct transport.

5.1 Temperature Dependence of the Lorentz Ratio

Temperature plays a crucial role in determining the dominant transport mechanism in an SET. At low temperatures, quantum effects such as co-tunneling significantly alter the energy transfer processes, while at higher temperatures, sequential tunneling becomes more prominent. Studying the Lorenz ratio as a function of temperature helps us understand how these mechanisms evolve with increasing thermal energy.

The above plot (fig.5.2) shows the theoretical study of how L/L_0 temperature evolves as temperature increases for different values of n_g . At high temperatures $(k_B >> E_C)$ the Lorenz ratio remains close to 1 for all n_g values, as thermal fluctuations dominate, and the SET behaves like a normal metal following the

Wiedemann-Franz law. As temperature decreases $(k_BT < E_C)$, deviations appear due to Coulomb blockade. The behavior depends on the gate position.

- At $n_g = 0.5$ (solid black line): The system is at a charge degeneracy point, allowing easy tunneling. The Lorenz ratio stays near 1 across all temperatures.
- At $n_g = 0.48$ (dotted) and $n_g = 0.4$ (dashed): The Lorenz ratio peaks before decreasing as sequential tunneling is suppressed and higher-order cotunneling dominates.
- At $n_g = 0$ (gray solid line)): The system is in Coulomb blockade, restricting electron flow. The Lorenz ratio rises significantly at low temperatures and settles at $L/L_0 = 9/5$ when co-tunneling becomes dominant.

In all the respective values of n_g , the L/L_0 rises at a specific temperature and reaches a maximum peak because at this temperature the charging energy gap (Δ_N) is quite high so, only the electron with high energy an tunnel through the island. These electrons carry more thermal energy per electron, increasing the heat-to-charge transport ratio. As a result, L/L_0 increases significantly away from degeneracy points.

In the lowest temperature regime, scattering becomes weakly energy-dependent, leading to a constant Lorenz ratio of 9/5. This confirms that quantum effects and electron interactions govern nano-scale thermal transport in SETs.

5.2 Experiments on Thermal transport through SETs

The theoretical understanding of thermal transport in Single-Electron Transistors (SETs), as discussed earlier, highlights the role of Coulomb interactions and quantum effects in modifying the Lorenz ratio. Following the theoretical discussion, experimental studies have been carried out to measure heat and charge transport in Single-Electron Transistors (SETs). These experiments test the Wiedemann-Franz law and explore deviations due to electron interaction. During thermal measurements, the SET is kept in a no-current state to measure only thermal conductance. Heat flow is analyzed as the source and island temperatures change. This is compared to electrical conductance. Electrons in the source reach thermal equilibrium due to fast interactions.

A Normal metal–Insulator–Superconductor (N–I–S) junction functions as a thermometer, with the voltage drop across the N–I–S junction reflecting the

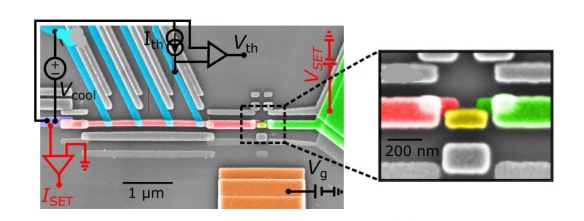


Figure 5.3: False-colored SEM image of the Asymmetric design[6] [pp.86-87] device. One of the blue colored component is the thermometer (extreme right side) and the other (extreme left side) is the cooler/heater. In the magnified image (left) red color indicates source, yellow is the metallic island and green is the drain. (Adapted from [5])

temperature of the normal metal. The biasing current is kept sufficiently small to ensure that no significant cooling occurs during the temperature measurement.

For cooling the source, we use the same process but with higher biasing current (but the voltage drop should be below Δ)so that significant number electron could tunnel into the superconductor with $E > \Delta$.

If the Biasing current is too high so that the energy due to the voltage drop across the N-I-S junction is greater than the superconductor energy gap(Δ), then the cooling mechanism is overwhelmed by heating, so the electron temperature T_e becomes greater than the phonon temperature T_b due to Joule heating.

Here, in the above fig.5.4(left) we can see that with the increase in cooling Voltage (V_{cool}) , which is applied to the superconductor lead (Al) (blue colored component in the extreme left in fig.5.3) below the energy gap (Δ) (within which cooper-pair exist) the temperature of the source also decreases under both the state of the gate (Off $n_g = 0$ as well as $On(n_g = 0.5)$). But this continuous till $V_{cool} \approx 190 \mu V$ which is the Voltage whose corresponding energy is equal to the energy gap(Δ). When $V_{cool} \approx 190 \mu V$, T_e reaches a minimum ($\approx 100 mK$), which is $\approx 50 mK$ below the bath temperature T_b .

When $V_{cool} > 190 \mu V$, T_e increases above T_b , means the system is now heating instead of cooling. This happens because at higher bias, Joule heating starts to dominate, leading to electron overheating.

Effect of gate induced charge n_q on cooling

The cooling is more effective when $n_g = 0$ (black dot) than when $n_g = 0.5$ (black circle). When $n_g = 0$, transport through the Single-Electron Transistor (SET) is blocked, reducing heat leakage, so more cooling is observed. When $n_g = 0.5$, the SET conducts more heat, reducing the cooling efficiency.

The two panels on the right of Fig. 2 demonstrate how the electronic temperature in the source can be modulated by controlling the charge state n_g and

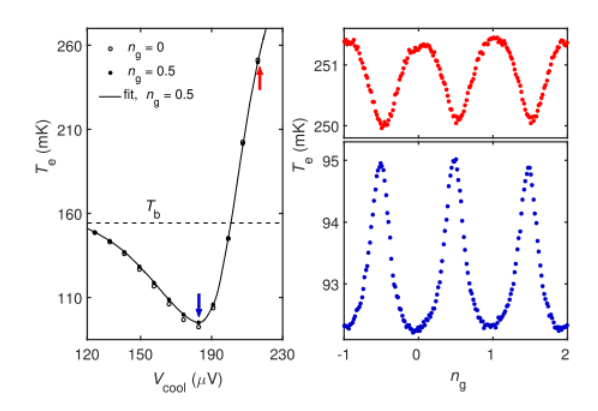


Figure 5.4: The left plot illustrates the variation of the electronic temperature T_e of sample B $(R_N = 52 \Omega)$ as a function of the cooler bias voltage V_{cool} . The right plot shows the dependence of T_e on the gate voltage: the top graph corresponds to the heating regime, while the bottom graph represents the cooling regime. (Adapted from [5]

).

adjusting V_{cool} .

Heating Regime (Top Panel, Red Dots) fig.5.4: At a specific high-bias setting of V_{cool} (marked by the red arrow in the left plot), the source experiences heating. This occurs as a result of high-energy electrons being injected from the superconducting cooler junction into the source. The energy added to the electronic bath increases temperature of electrons T_e and the effect is modulated by gate induced charge n_g . The periodic oscillations in T_e arise from Coulomb blockade effects, which influence the tunneling rates.

Cooling Regime (Bottom Panel, Blue Dots)fig.5.4: At a different bias condition (blue arrow in the left plot), V_{cool} is set such that high-energy electrons are selectively removed from the source. This leads to a net cooling effect, reducing T_e . Similar to the heating case, the effect is modulated by n_g and periodic oscillations in temperature are observed.

5.2.1 Thermoelectric Conductance Characteristics of a SET

In figure 5.5 ,we can see the measured thermal conductance (k) and charge conductance (σ) of a Single Electron Transistor (SET) as a function of the induced gate charge (n_g) . The measurements were taken at low temperatures for two different samples. Sample A(left panel)- Tunnel resistance: $(164k\Omega)$ and Sample B(right panel)-Tunnel resistance: $(52k\Omega)$. The goal of this measurement is to study how heat and charge transport behave in a SET and whether the

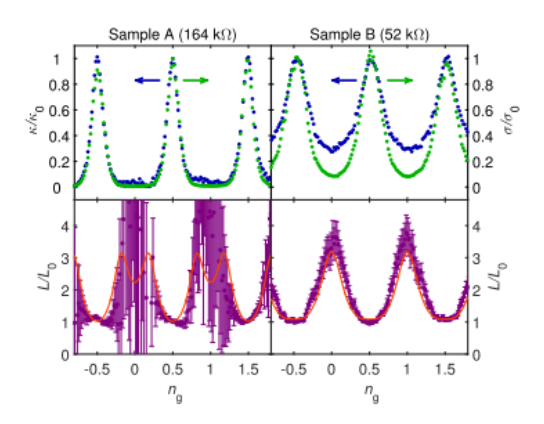


Figure 5.5: The thermal conductance (represented by blue dots) and charge conductance (depicted by green dots) of the SET are shown at a bath temperature of 132 mK (left, sample A) and 152 mK (right, sample B), measured relative to the conductances observed in the gate-open configuration. (Adapted from[5])

Wiedemann-Franz law holds.

The top plots show how the thermal conductance k (blue dots) and charge conductance σ (green dots) vary with the gate charge n_g . The charge conductance σ exhibits periodic oscillations as a function of n_g , which is a characteristic feature of Coulomb charging phenomena in a nanoscale single-electron device (SET). The thermal conductance k follows a similar oscillatory behavior but does not decrease as sharply as the charge conductance within the Coulomb blockade regime.

When $(n_g) = 0.5$ or any half-integral value(gate-open state or degenerate state), both conductance reaches their maximum as well as the same values, which means that at these values, the SET obeys Weidemann-Franz law. But when $n_g = 0$ or any integral value (Coulomb blockade region), charge conductance is strongly suppressed, and thermal conductance also decreases but remains non-zero. This means that in the Coulomb blockade regime, charge transport is significantly reduced, but heat transport is still present due to energy exchange processes.

Sample A (left) shows a stronger Coulomb blockade effect than Sample B (right). This is because Sample A has a higher tunnel resistance, which restricts electron flow more strongly.

The bottom plots of fig.5.5 display the Lorenz ratio (L/L_0) , which helps in determining whether the Wiedemann-Franz law holds in the SET. The red line represents the theoretical prediction from Ref. [14]. The purple dots show the experimental data.

When $n_g = 0.5$ (gate-open state), the Lorenz ratio is close to 1, indicating that

the Wiedemann–Franz law is satisfied. This implies that electrons carry both heat and charge as expected. On the other hand, in the regime characterized by Coulomb blockade ($n_g = 0$), the Lorenz number deviates significantly from 1, indicating a breakdown of the standard relationship between heat and charge transport, likely due to additional interactions affecting energy flow.

Sample A exhibits stronger deviations from the Wiedemann–Franz law compared to Sample B. This is attributed to its higher tunnel resistance, which enhances the effects of electron–electron interactions. These observations confirm that the Wiedemann–Franz law holds in the gate-open state but breaks down in the Coulomb blockade regime due to strong electronic correlations.

Conclusion

In this thesis, I have studied the theoretical aspects of electron transport in nanoscale systems, with a focus on Single-Electron Transistors (SETs) and quantum dots (QDs). At small dimensions, electrons do not behave the same way as they do in larger devices. Quantum effects such as tunneling, Coulomb blockade, and discrete energy levels become very important and strongly influence how current flows.

The study began with SETs based on metallic islands, where the transport of electrons is governed by charging energy. Electrons can only move through the device if energy conditions are met, which can be controlled using gate voltage. I then studied SETs that use quantum dots, where electrons are even more tightly confined, and the energy levels become discrete. This leads to distinct features in transport behavior, such as Coulomb diamonds and regular conductance oscillations.

I also examined more advanced transport processes such as co-tunneling and the Kondo effect. These effects become important when simple tunneling is not allowed, especially at low temperatures. They help explain how electrons can still move through the device even when direct paths are blocked.

In addition to charge transport, this thesis also explored thermal transport in Single-Electron Devices. At this scale, electrons also carry heat, and their behavior can change depending on gate voltage, temperature, and energy level alignment. The study showed that common classical laws, like the Wiedemann–Franz law, may not always apply under these conditions. This is important when designing small devices that need to be both energy-efficient and thermally stable.

Overall, this work gave me a better understanding of how electrons move and interact in small systems. It also showed how theoretical models, combined with results from experiments, can help explain the unique behavior of electrons in nanoscale electronics. These insights are useful for the future development of low-power and high-performance electronic devices.

Appendix A

Derivation of Energy cost for tunneling

A.0.1 Total charging energy:

The overall electrostatic energy associated with a small metallic island in a Single-Electron Transistor (SET), where the island has N excess electrons, is given by:

$$E_{\text{total}} = \frac{N^2 e^2}{2C} \tag{A.1}$$

Where:

- e denotes the fundamental unit of electric charge.
- $C = C_1 + C_2 + C_g$ represents the combined capacitance associated with the island, comprising connections to the source (C_1) , drain (C_2) , and gate (C_g) .

Gate-Induced Charge: The gate induces a charge $Q_g = C_g V_g$, and this can be expressed in terms of a dimensionless gate charge n_g as:

$$n_g = \frac{C_g V_g}{e} \tag{A.2}$$

Thus, the gate-induced charge $n_g e$ modifies the total energy of the system.

Total Electrostatic Energy with Gate-Induced Charge: The total electrostatic energy of the system, accounting for the gate-induced charge, is:

$$E_{\text{charging}} = \frac{N^2 e^2}{2C} - Ne\phi_g$$

$$E_{\text{charging}} = \frac{N^2 e^2}{2C} - \frac{Nn_g e^2}{C}$$
(A.3)

where: The term $\frac{N^2e^2}{2C}$ represents the charging energy of the island with n excess electrons. The term $\frac{Nn_ge^2}{C}$ represents the energy of the Dot due to the gate-induced charge n_g . $\phi_g = V_g = \frac{n_ge^2}{C}$

Energy Change Due to Tunneling

Now, we calculate the energy cost for tunneling an electron onto the island $(\Delta E_{i,N}^+)$ or off the island $(\Delta E_{i,N}^-)$.

1. Energy Cost for Tunneling an Electron Onto the Island: When an electron is added to the island, the count of surplus electrons increases from N to N+1. The required energy for adding an electron $(\Delta E_{i,N+})$ is the difference in electrostatic energy between the (N+1) electron state and the N electron state:

$$\Delta E_{iN}^+ = E(N+1) - E(N)$$

Substituting the expression for E(N+1) and E(N):

$$E(N+1) = \frac{(N+1)^2 e^2}{2C} - \frac{(N+1)n_g e^2}{C}$$
$$E(N) = \frac{N^2 e^2}{2C} - \frac{Nn_g e^2}{C}$$

Now, calculating the energy difference:

$$\Delta E_{i,N}^{+} = \left(\frac{(N+1)^2 e^2}{2C} - \frac{(N+1)n_g e^2}{C}\right) - \left(\frac{N^2 e^2}{2C} - \frac{Nn_g e^2}{C}\right)$$

$$\Delta E_{i,N}^{+} = \left(\frac{(N^2 + 2N + 1)e^2}{2C} - \frac{(Nn_g e^2 + n_g e^2)}{C}\right) - \left(\frac{N^2 e^2}{2C} - \frac{Nn_g e^2}{C}\right)$$

Now, after simplifying, we get:

$$\Delta E_{i,N}^{+} = \frac{e^2}{C} \left(N - n_g + \frac{1}{2} \right) \tag{A.4}$$

2. Energy Cost for Tunneling an Electron Off the Island: When an electron is removed from the island, the number of excess electrons changes from N to (N-1). The energy cost for removing an electron $(\Delta E_{i,N}^-)$ is the difference in electrostatic energy between the N-1-electron state and the N electron state:

$$\Delta E_{i,N}^- = E(N-1) - E(N)$$

Substituting the expression for E(N-1) and E(N):

$$E(N-1) = \frac{(N-1)^2 e^2}{2C} - \frac{(N-1)n_g e^2}{C}$$
$$E(n) = \frac{N^2 e^2}{2C} - \frac{Nn_g e^2}{C}$$

Now, calculating the energy difference:

$$\Delta E_{i,N}^{-} = \left(\frac{(N-1)^2 e^2}{2C} - \frac{(N-1)n_g e^2}{C}\right) - \left(\frac{N^2 e^2}{2C} - \frac{Nn_g e^2}{C}\right)$$

$$\Delta E_{i,N}^{-} = \left(\frac{(N^2 - 2N + 1)e^2}{2C} - \frac{(Nn_g e^2 - n_g e^2)}{C}\right) - \left(\frac{N^2 e^2}{2C} - \frac{Nn_g e^2}{C}\right)$$

Now, after simplifying further, we get:

$$\Delta E_{i,N}^{-} = -\frac{e^2}{C} \left(N - n_g - \frac{1}{2} \right) \tag{A.5}$$

3. Incorporating Bias Voltage: In addition to the charging energy, we must account for the bias voltage V_b applied across the tunnel junctions. A portion of the total bias voltage, denoted as $V_{b,i} = k_i V_b$, falls across junction i, where k_i is the fraction determined by the capacitance.

For a symmetric SET, $k_1 = k_2 = \frac{1}{2}$.

Thus, we add a term $eV_{b,i}$ to account for the energy cost associated with the bias voltage.

The energy cost for adding an electron:

$$\Delta E_{i,n}^+ + eV_{b,i}$$

The energy cost for removing an electron:

$$\Delta E_{i,n}^- - eV_{b,i}$$

4. Final Energy Expression:

For tunneling an electron onto the island:

$$\Delta E_{i,n}^{+} = \frac{e^2}{C} \left(n - n_g + \frac{1}{2} \right) + eV_{b,i}$$
 (A.6)

For tunneling an electron off the island:

$$\Delta E_{i,n}^{-} = \frac{e^2}{C} \left(-n + n_g + \frac{1}{2} \right) - eV_{b,i}$$
 (A.7)

Now, combining the energy cost for tunneling onto or off the island, i.e. eq^n (A.6) & (A.7) , we get:

$$\Delta E_{i,n}^{\pm} = \pm 2E_c \left(n - n_g \pm \frac{1}{2} \right) \pm eV_{b,i}$$

This is the energy cost for tunneling electrons onto and off the island.

Appendix B

Derivation of the chemical potential of Quantum Dot(QD):

Derivation of the expression We know

$$E_{\text{total}}(N) = \sum_{P=1}^{N} \varepsilon_P + E_{el}(N)$$
$$= \sum_{P=1}^{N} \varepsilon_P + \frac{(N_e)^2}{2C} - Ne \ \phi_{\text{ext}}$$

This is the electrostatic potential energy of the QD due to N particles. putting (N+1) in place of N in the above equation we get,

$$E_{\text{total}}(N+1) = \sum_{p=1}^{N+1} \varepsilon_p + \frac{(N+1)^2 e^2}{2c} - (N+1)e\phi_{ext}$$

This is the electrostatic potential energy of the QD due to (N+1) particles.

Now, The chemical potential necessary for the addition of an electron to the (N+1)th energy level, which is a vacant level with energy, $\varepsilon_{(N+1)}$ is given by:

$$\mu(N) = E_{\text{total}}(N+1) - E_{\text{total}}(N)$$
(B.1)

Now, putting the value of $E_{\text{total}}(N)$ and $E_{\text{total}}(N+1)$ from the above two expressions, we get:

$$\begin{split} \mu(N) &= \sum_{p=1}^{N+1} \varepsilon_p + \frac{(N+1)^2 e^2}{2C} + (N+1) e \phi_{ext} - \sum_{p=1}^{N} \varepsilon_p - \frac{N^2 e^2}{2c} + N e \phi_{ext} \\ \mu(N) &= \varepsilon_{N+1} + \frac{N^2 e^2}{2c} + \frac{e^2}{2c} + \frac{2N e^2}{2c} - N e \phi_{ext} - e \phi_{e_{ext}} - \frac{N^2 e^2}{2c} + N e \phi_{ext} \\ \mu(N) &= \varepsilon_{N+1} - e \phi_{ext} + (N+\frac{1}{2}) \frac{e^2}{c} \end{split}$$

This is the total energy required for the tunneling of an electron onto the QD.

Appendix C

Derivation of the expression of the slope of coulumb diamond:

1.Derivation of
$$V_b = \beta V_g + K$$
 and $V_b = -\beta V_g + K$

The linear equation of +ve and -ve edges of the Coulamb diamond can be find out in the following way

The expression for the chemical potential of the source ($\mu_{\rm s}$) is

$$\mu_s = \mu_0 + ev_b$$

where: μ_0 is the intrinsic electrochemical potential at given temperature without biasing and v_q . eV_b is the potential energy due to the biasing.

Let us consider the drain to be grounded.

Now, the chemical potential of the dot, $\mu_d = \mu_0 + eV_{dot}$ where:

$$V_{dot}$$
 or $\phi_{ext,i} = \sum_i \frac{C_i}{C} V_{ext,i}$ and $V_{dot} = \frac{C_s V_b}{c} + \frac{C_g V_g}{c} + \frac{C_d V_d}{c}$

$$since, V_d = 0$$

$$so, V_{dot} = \frac{C_s V_b}{c} + \frac{C_g C_g}{c}$$

$$\therefore \mu_{dot} = \mu_0 + e\left(\frac{C_s V_b + C_g V_g}{C}\right)$$

$$C = C_s + C_d + C_g$$

Now for the $+\mathbf{ve}$ edges condition we use the balancing equation since at this condition the $\mu_{dot}\& \mu_s$ align with each other. So, thus the balancing condition is given by:

$$\mu_{dot} = \mu_s (\text{ Boundary condition })$$

$$\Rightarrow \mu_o + eV_b = \mu_0 + \left(\frac{C_g V_b + C_g V_g}{C} \right)$$

$$\Rightarrow CV_b = C_s V_b + C_g V_g$$

$$\Rightarrow (C - C_s) V_b = C_g V_g$$

$$\Rightarrow (C_s + C_d + C_g - C_s) V_b = C_g V_g$$

$$\Rightarrow V_b = \left(\frac{C_g}{C_d + C_g} \right) V_g + K$$

$$\therefore V_b = \beta V_g + K$$
(C.1)

Where $\beta = \frac{C_g}{C_d + C_g} \rightarrow \text{slope of } + \mathbf{ve} \text{ edge.}$

K is a constant.

Now for the **-ve** slope we use similar balancing condition since now $\mu_{dot}\&\mu_d$ align with each other. So, the balancing condition is given by:

$$\mu_{d} = \mu_{0}(\text{ since}, V_{d} = 0)$$
so,
$$\mu_{d} = \mu_{dot}$$

$$\Rightarrow \mu_{0} = \mu_{0} + eV_{dot}$$

$$\Rightarrow V_{dot} = 0 \Rightarrow \frac{C_{s}V_{b}}{C} + \frac{C_{g}V_{g}}{C} = 0$$

$$\Rightarrow C_{s}V_{b} = -C_{g}V_{g}$$

$$\Rightarrow V_{b} = -\frac{C_{g}}{V_{s}}V_{g} + K$$

$$\therefore V_{b} = -\beta'V_{g} + K$$
(C.2)

where : $\beta' = \frac{C_g}{C_s}$ and K is a constant.

here, μ_0 is the intrinsic chemical potential which is same for source(s),drain(d)an dot because they are made of same metal. (Without biasing and V_g and at same temperature they are at equilibrium. There is no potential difference.)

Thus,
$$B = \frac{C_g}{C_d + C_y}$$
, $B' = \frac{C_9}{C_S}$

The constant K denotes the intrinsic potential of the quantum dot when no external voltage is applied.

The characteristic slopes of the Coulomb diamond uniquely reflect the properties of the quantum dot.

2. Derivation of the ratio $\frac{C_d}{C_S}$:

The slopes provide us the information about the asymmetry in the capacitive coupling of the dot to source & drain. Which is given by

we know

$$\beta = \frac{C_g}{C_d + C_g} \tag{C.3}$$

$$\beta' = \frac{C_g}{C_q} \tag{C.4}$$

From equation (C.3),

$$\Rightarrow \beta = \frac{C_g}{C_d + C_g}$$

$$\Rightarrow \beta (C_d + C_g) = C_g$$

$$\Rightarrow \beta C_d = C_g (1 - \beta)$$

$$\Rightarrow C_d = C_g \frac{(1 - \beta)}{\beta}$$

we have in equation (C.4)

$$\beta' = \frac{C_g}{C_s}$$

$$\Rightarrow C_s = \frac{C_g}{\beta'}$$

$$\frac{C_d}{C_s} = \frac{\frac{C_g(1-\beta)}{C_g}}{\frac{C_g}{\beta'}} = \beta' \left(\frac{1}{\beta} - 1\right)$$

$$\therefore \frac{C_d}{C_s} = \beta' \left(\frac{1}{\beta} - 1\right)$$

- If $\frac{C_d}{C_s} = 1$, the coupling is symmetry meaning the quantum dot is equally coupled to both the source and the drain. $\frac{C_d}{C_s} > 1$, then the quantum dot becomes preferentially connected to the drain electrode.
- If $\frac{C_d}{C_s} < 1$, then the quantum dot is more effectively linked to the source electrode.

3.Derivation of $\alpha = \frac{C_g}{C}$:

The lever arm α , or gate coupling factor, represents the rate at which the dot's chemical potential changes with gate voltage, expressed as $\alpha = \frac{\Delta \mu}{\Delta V_g}$. It can be determined directly from the slopes of the Coulomb diamond edges as,

we have,

$$\beta = \frac{C_g}{(C_d + C_g)} and \beta I = \frac{C_g}{C_s} . (C_d + C_g)$$

Now taking the reciprocal of both terms, side by side we get:

$$\Rightarrow \frac{1}{\beta} = \frac{C_d + C_g}{C_g} and \frac{1}{\beta \prime} = \frac{C_s}{C_g}$$

Now summing both the reciprocal terms we get:

$$\frac{1}{\beta} + \frac{1}{\beta \prime} = \frac{C_s + C_d + C_g}{C_g} = \frac{C}{C_g} = \frac{1}{\alpha}$$

Thus,

$$\alpha = \frac{C_g}{C} = \frac{1}{\frac{1}{\beta} + \frac{1}{\beta \prime}}$$

This is the required expression of $\alpha.[4]$

Bibliography

- [1] T. A. Costi, A. C. Hewson, and V. Zlatić. Transport coefficients of the anderson model via the numerical renormalization group. *Journal of Physics: Condensed Matter*, 6(13):2519, mar 1994.
- [2] S. De Franceschi, S. Sasaki, J. M. Elzerman, W. G. van der Wiel, S. Tarucha, and L. P. Kouwenhoven. Electron cotunneling in a semiconductor quantum dot. *Phys. Rev. Lett.*, 86:878–881, Jan 2001.
- [3] S De Franceschi, S Sasaki, JM Elzerman, WG Van Der Wiel, S Tarucha, and Leo P Kouwenhoven. Electron cotunneling in a semiconductor quantum dot. *Physical review letters*, 86(5):878, 2001.
- [4] Debika Debnath and Paramita Dutta. Gate-tunable josephson diode effect in rashba spin-orbit coupled quantum dot junctions. *Phys. Rev. B*, 109:174511, May 2024.
- [5] B. Dutta, J. T. Peltonen, D. S. Antonenko, M. Meschke, M. A. Skvortsov, B. Kubala, J. König, C. B. Winkelmann, H. Courtois, and J. P. Pekola. Thermal conductance of a single-electron transistor. *Phys. Rev. Lett.*, 119:077701, Aug 2017.
- [6] Bivas Dutta. Energetics in metallic-island and quantum-dot based single-electron devices. Theses, Université Grenoble Alpes, November 2018.
- [7] Bivas Dutta, J. Peltonen, D. Antonenko, M. Meschke, Mikhail Skvortsov, B. Kubala, J. König, C. Winkelmann, H. Courtois, and J. Pekola. Thermal conductance of a single-electron transistor. *Physical Review Letters*, 119:077701, 08 2017.
- [8] Wipsar Dwandaru and Denny Darmawan. Towards the dynamics of coulomb blockade in quantum dot via the totally asymmetric simple exclusion process with a single site. *Advanced Studies in Theoretical Physics*, 10:23–32, 01 2016.

- [9] D. Goldhaber-Gordon, J. Göres, M. A. Kastner, Hadas Shtrikman, D. Mahalu, and U. Meirav. From the kondo regime to the mixed-valence regime in a single-electron transistor. *Phys. Rev. Lett.*, 81:5225–5228, Dec 1998.
- [10] Hermann Grabert and Michel H Devoret. Single charge tunneling: Coulomb blockade phenomena in nanostructures, volume 294. Springer Science & Business Media, 2013.
- [11] Marc A Kastner. The single-electron transistor. Reviews of modern physics, 64(3):849, 1992.
- [12] Jun Kondo. Resistance minimum in dilute magnetic alloys. *Progress of Theoretical Physics*, 32(1):37–49, 07 1964.
- [13] Leo P. Kouwenhoven, Charles M. Marcus, Paul L. McEuen, Seigo Tarucha, Robert M. Westervelt, and Ned S. Wingreen. *Electron Transport in Quantum Dots*, pages 105–214. Springer Netherlands, Dordrecht, 1997.
- [14] Björn Kubala, Jürgen König, and Jukka Pekola. Violation of the wiedemann-franz law in a single-electron transistor. *Phys. Rev. Lett.*, 100:066801, Feb 2008.

Msc_Thesis.pdf

| ORGANLITY REPORT | | |
|--|----------|--|
| 14% 14% 12% 2% SIMILARITY INDEX INTERNET SOURCES PUBLICATIONS STUDEN | T PAPERS | |
| PRIMARY SOURCES | | |
| tel.archives-ouvertes.fr | 2% | |
| 2 hdl.handle.net Internet Source | 1% | |
| Submitted to Indian Institute of Technology Indore Student Paper | 1% | |
| 4 123dok.net Internet Source | <1% | |
| 5 docslib.org | <1% | |
| 6 meso.seas.harvard.edu | <1% | |
| 7 www.repository.cam.ac.uk | <1% | |
| 8 portal.research.lu.se | <1% | |
| opus.bibliothek.uni-wuerzburg.de | <1% | |
| 10 www.scribd.com | <1% | |
| Electron Transport in Quantum Dots, 2003. | <1% | |
| www.repo.uni-hannover.de | <1% | |
| | | |

| 13 | research.tue.nl | <1% |
|----|---|-----|
| 14 | sciencedocbox.com Internet Source | <1% |
| 15 | diglib.tugraz.at | <1% |
| 16 | d-nb.info Internet Source | <1% |
| 17 | digital.csic.es | <1% |
| 18 | Ireneusz Weymann, Jürgen König, Jan Martinek, Józef Barnaś, Gerd Schön. "Tunnel magnetoresistance of quantum dots coupled to ferromagnetic leads in the sequential and cotunneling regimes", Physical Review B, 2005 Publication | <1% |
| | | |
| 19 | Mesoscopic Electron Transport, 1997. Publication | <1% |
| 20 | Mesoscopic Electron Transport, 1997. Publication Kushwaha, M.S "Plasmons and magnetoplasmons in semiconductor heterostructures", Surface Science Reports, 200103 Publication | <1% |
| = | Kushwaha, M.S "Plasmons and magnetoplasmons in semiconductor heterostructures", Surface Science Reports, 200103 | |
| 20 | Kushwaha, M.S "Plasmons and magnetoplasmons in semiconductor heterostructures", Surface Science Reports, 200103 Publication Natalya A. Zimbovskaya. "Transport Properties of Molecular Junctions", Springer Science and Business Media LLC, 2013 | <1% |
| 20 | Kushwaha, M.S "Plasmons and magnetoplasmons in semiconductor heterostructures", Surface Science Reports, 200103 Publication Natalya A. Zimbovskaya. "Transport Properties of Molecular Junctions", Springer Science and Business Media LLC, 2013 Publication Submitted to University of Sheffield | <1% |

| | Internet Source | <1% |
|----|---|-----|
| 25 | fisica.cab.cnea.gov.ar | <1% |
| 26 | yujunmao1.github.io | <1% |
| 27 | Akman, Nurten. "Electron-Electron Interactions in a Two Dimensional Quantum Dot.", Middle East Technical University (Turkey), 2024 Publication | <1% |
| 28 | Topics in Applied Physics, 2008. | <1% |
| 29 | "New Materials for Thermoelectric Applications: Theory and Experiment", Springer Science and Business Media LLC, 2013 Publication | <1% |
| 30 | S. Gustavsson, R. Leturcq, M. Studer, I. Shorubalko, T. Ihn, K. Ensslin, D.C. Driscoll, A.C. Gossard. "Electron counting in quantum dots", Surface Science Reports, 2009 | <1% |
| 31 | Khan, Saba Mehsar. "A Vibrating Carbon Nanotube Probe to Study Superfluid 4He", Lancaster University (United Kingdom), 2025 | <1% |
| 32 | NanoScience and Technology, 2014. | <1% |
| 33 | www.theorie.physik.uni-muenchen.de | <1% |
| 34 | Pouse, Winston. "Quantum Simulation Using Hybrid Metal-Semiconductor Islands", | <1% |

Stanford University, 2023

| 35 | smartech.gatech.edu Internet Source | <1% |
|----|--|-----|
| 36 | Submitted to Royal Holloway and Bedford New College Student Paper | <1% |
| 37 | Springer Series in Solid-State Sciences, 2007. Publication | <1% |
| 38 | eprints.lancs.ac.uk | <1% |
| 39 | nbi.ku.dk Internet Source | <1% |
| 40 | www.science.org | <1% |
| 41 | Scheibner, Ralf. "Thermoelectric Properties of Few-Electron Quantum Dots", Universität Würzburg, 2008. | <1% |
| 42 | www.arxiv-vanity.com | <1% |
| 43 | Gulzat Jaliel. "Thermoelectric properties of a quantum dot", Elsevier BV, 2021 | <1% |
| 44 | Submitted to Indian Institute of Management, Indore Student Paper | <1% |
| 45 | dspace.mit.edu | <1% |
| 46 | sites.bu.edu Internet Source | <1% |
| | | |

| 47 | A. D. Armour. "Classical dynamics of a nanomechanical resonator coupled to a single-electron transistor", Physical Review B, 03/2004 Publication | <1% |
|----|--|-----|
| 48 | Gaaß, Markus. "The Kondo effect in single wall carbon nanotubes with ferromagnetic contacts", Publikationsserver der Universität Regensburg, 2012. Publication | <1% |
| 49 | Karyn Le Hur. "Capacitance of a quantum dot from the channel-anisotropic two-channel Kondo model", Physical Review B, 04/2002 Publication | <1% |
| 50 | Pelliccione, Matthew. "Local Imaging of High Mobility Two-dimensional Electron Systems with Virtual Scanning Tunneling Microscopy.", Stanford University, 2020 | <1% |
| 51 | Springer Series in Materials Science, 1994. | <1% |
| 52 | Su, Zhaoen. "Andreev Bound States in Superconductor-Quantum Dot Chains.", University of Pittsburgh, 2018 Publication | <1% |
| 53 | Zhang, X.M "Thermopower of a multilevel quantum dot coupled with leads in Coulomb blockade", Physics Letters A, 20080414 Publication | <1% |
| 54 | ricerca.sns.it | <1% |
| 55 | ris.utwente.nl | <1% |

| 56 | Egger, Reinhold, Alex Zazunov, and Alfredo Levy Yeyati. "Interaction Effects on Transport in Majorana Nanowires", Topological Insulators, 2015. | <1% |
|----|--|-----|
| 57 | T. A. Costi, V. Zlatić. "Thermoelectric transport through strongly correlated quantum dots", Physical Review B, 2010 | <1% |
| 58 | lup.lub.lu.se | <1% |
| 59 | theses.fr Internet Source | <1% |
| 60 | www.iqst.ca Internet Source | <1% |
| | | |
| | le quotes On Exclude matches < 15 words le bibliography On | |